Aqueous AC-Line Filtering Electrochemical Capacitors Featuring 2.5-V Voltage Window and Kilohertz Response Using Boron-Doped Diamond Nanoarrays

Peer-reviewed author version

Chen, Bin; Zhai, Zhaofeng; Zhang , Chuyan; Li, Junyao; Zheng, Shuailong; Liu , Lusheng; Zhang, Wenjun; Jiang , Xin; Yang , Yang; YANG, Nianjun & Huang, Nan

(2025) Aqueous AC-Line Filtering Electrochemical Capacitors Featuring 2.5-V Voltage Window and Kilohertz Response Using Boron-Doped Diamond Nanoarrays. In: Advanced functional materials,.

DOI: 10.1002/adfm.202509964
Handle: http://hdl.handle.net/1942/46368

Aqueous AC-Line Filtering Electrochemical Capacitors Featuring 2.5-V Voltage Window and Kilohertz Response Using Boron-Doped Diamond Nanoarrays

Bin Chen,[a] Zhaofeng Zhai,[a,b] Chuyan Zhang,[a] Junyao Li,[a] Shuailong Zheng,[a,b] Lusheng Liu,[a] Wenjun Zhang,[c] Xin Jiang,[a] Yang Yang,[d,] Nianjun Yang,[e,]* Nan Huang,[a,b,]**

a. Shenyang National Laboratory for Materials Science, Institute of Metal Research, Chinese Academy of Sciences, Shenyang 110016, China
b. School of Materials Science and Engineering, University of Science and Technology of China, Shenyang 110016, China
c. Department of Materials Science and Engineering, and Center of Super-Diamond and Advanced Films (COSDAF), City University of Hong Kong, Kowloon, Hong Kong SAR, China
d. Advanced Energy Storage Technology Research Center, Shenzhen Institute of Advanced Technology, Chinese Academy of Sciences, Shenzhen 518055, China
e. Department of Chemistry & IMO-IMOMEC, Hasselt University, Diepenbeek 3590, Belgium

* Corresponding Author: yang.yang1@siat.ac.cn; nianjun.yang@uhasselt.be; nhuang@imr.ac.cn.

Abstract

Electrochemical capacitors show great promise in alternate current (AC) line filtering for modern miniaturized electronics, yet their widespread adoption is significantly hindered by limited voltage window and slow response. Herein, an aqueous electrochemical capacitor for wide-voltage and ultrafast-response filtering is developed using the boron-doped diamond electrodes that feature both the ultra-wide potential window of 2.93 V and vertical-oriented nanoarray architecture. This capacitor exhibits a wide voltage window up to 2.5 V larger than those of reported aqueous filtering capacitors to date and a high-frequency response capability with a characteristic frequency f_0 = 3338 Hz, as well as a phase angle of −80.4° and a high specific energy density of 365.6 μFV^2/cm^2 at 120 Hz. These superior properties enable effective ripple smoothing of rectified AC signals with complex waveforms, high frequency (60-1000 Hz), and large voltage amplitudes up to 5 V. This work presents an enlightening strategic design of filtering electrochemical capacitors featuring wide voltage windows and high-frequency response, thereby providing an effective solution to address key challenges in the integration and miniaturization of next-generation electronic devices.

Keywords: electrochemical capacitor, boron-doped diamond, wide voltage window, high-frequency response, AC-line filtering

1. Introduction

As a key component in an alternating current (AC) line filtering circuit, filtering capacitor is used to smooth the rectified AC waveform [1,2]. With increasing demands for the integration and miniaturization of electronic devices, it is necessary for the filtering capacitor to operate with high capacitance density and within a compact form. However, aluminum electrolytic capacitors (AECs), commonly used as conventional filtering capacitors for AC-line filtering, fail to meet these demands due to their low capacitance density and bulky size.

Electrochemical capacitors (ECs), based on the principle of electrochemical double layer or pseudocapacitance, are considered as promising candidates for next-generation filtering capacitors because of their high capacitance density and compact size, provided they demonstrate a high-frequency response.[3-10] In 2010, Miller et al demonstrated that the high-frequency response characteristic, comparable to that of AEC, can be achieved in ECs by constructing vertical-oriented or open porous structures to enhance ionic kinetics in ECs electrodes.[11] To date, filtering ECs based on vertical or open porous graphene [12-19], carbon nanotubes [4,7,8,20-22], and Mxene[23-25] and conducting polymer [3,5,26] electrodes have been reported to further achieve increased capacity and comparable high-frequency response. However, most of these ECs can only operate within a low voltage range (~1 V) using aqueous electrolytes, because of narrow stable potential window of water on these electrode materials surface. Although the utilization of organic electrolytes [27-29], water-in-salt [30] and room-temperature ionic liquids [31] in ECs enables a relatively wider voltage range (2-4 V), their ionic conductivities are much lower than those of aqueous electrolytes, resulting in slower ion diffusion kinetics and a significantly reduced high-frequency response. Many efforts have been made to enhance the working voltage of aqueous filtering ECs by optimizing the device structure, particularly through the utilization of diverse positive and negative electrode materials (i.e., asymmetric capacitors). [5,6,23] However, despite these endeavors, the achieved working voltage thus far remains below 2 V.

Boron-doped diamond (BDD), as a unique electrode material, enables the construction of aqueous ECs with a wide operative voltage [32]. This is due to the fact that the electrochemical decomposition reaction of water (hydrogen evolution or oxygen evolution) on the BDD electrode surface requires a significant overpotential, which can be attributed to the absence of electrochemically active sites on

the BDD surface [33]. For instance, the microcrystalline BDD electrode with a boron concentration of 5×10^{20} cm^{-3} exhibits an extended electrochemical potential window of 3.1 V in aqueous electrolyte, surpassing those of sp^2 carbon materials or other electrode materials used in ECs.[34-38] Therefore, the achievement of overcoming the operating voltage limitation in existing aqueous filtering ECs can be envisioned through the construction of BDD electrodes with a vertical orientation or an open porous structure.

In this work, we report an aqueous AC-line filtering EC with a wide workable window and a kilohertz response using BDD nanoarrays (denoted as BDD-NAs) as the electrode. These BDD-NAs, with an extended electrochemical potential window of 2.93 V similar to classical microcrystalline BDD and a vertically oriented porous structure that enables ultra-fast ion diffusion kinetics, were prepared by using the hot-filament chemical vapor deposition (HFCVD) and the reactive ion etching (RIE) technique. Furthermore, a symmetrical EC unit was fabricated based on BDD-NAs achieving a wide operational window of 2.5 V and an ultra-fast response up to 3338 Hz. Consequently, the wide operational window and ultra-fast response of such an EC unit enable the great performance in smoothing 60-1000 Hz AC-line inputs with a high voltage amplitude of 5 V.

2. Results and Discussion

2.1. Design and Preparation of the BDD-NAs electrode

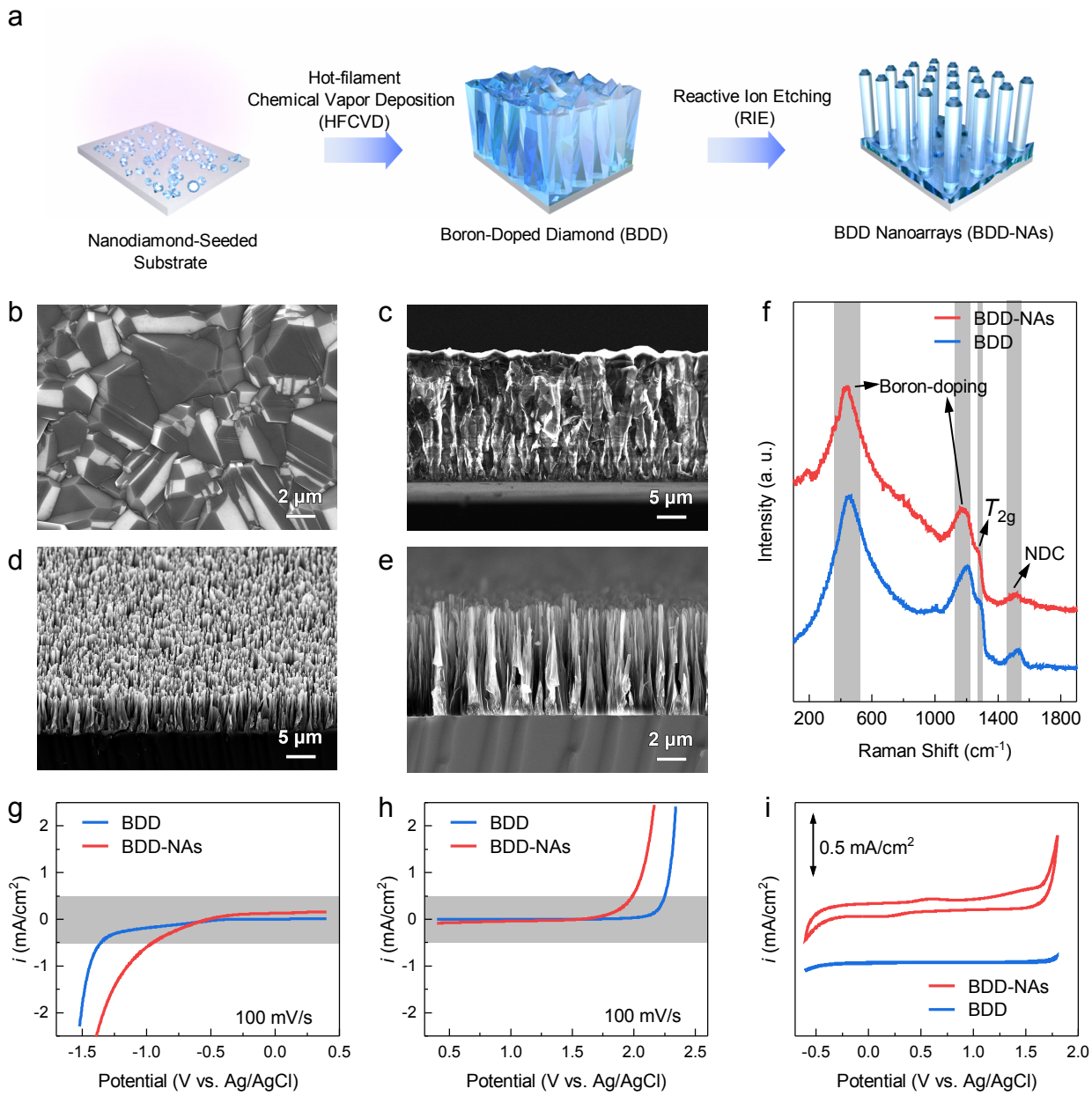

Figure 1. Preparation and characteristic of the BDD-NAs electrode. (a) schematic illustration of preparation process of BDD-NAs; (b) Top view and (c) cross-sectional view SEM images of the BDD; (d) Oblique view, and (e) cross-sectional view SEM images of BDD-NAs; (f) Raman spectra of the BDD and BDD-NAs excited at 532 nm; (g) Negative and (h) positive polarization scanning LSV curves of BDD and BDD-NAs at 100 mV/s.; (i) CV curves of BDD and BDD-NAs at 100 mV/s.

The preparation process of BDD-NAs electrode is schematically illustrated in **Figure 1a**. Initially, a polycrystalline BDD film was grown using hot-filament chemical vapor deposition (HFCVD) technique. In this process, precursor gases including methane (CH_4), hydrogen (H_2) and 1% trimethyl-borane (TMB) in H_2 were passed into a vacuum chamber and then activated by the thermal field of the hot tantalum filaments (> 2000). As a result, these gases dissociated to form a high energy-state plasma consisting of uniformly distributed atomic or active groups. These active groups, containing boron and carbon atoms, were then uniformly deposited onto a Si substrate with diamond seeds for BDD growth (see Table S1, Supporting Information for detailed information). The resulting BDD film exhibited micron-sized crystals with an average grain size ranging from 3-5 μm and had a thickness of 18 μm (**Figure 1b-c**). The X-ray photoelectron spectroscopy (XPS) indicate that the boron concentration in our BDD film reaches a magnitude of 10^{21} atom/cm^3 (Figure S1, Supporting Information). The high boron concentration of our BDD film indicates the presence of a Mott insulator-metal transition, wherein the energy level resulting from boron doping at the top of the valence band expands and overlaps with the valence band, thereby leading to a metallic-like electrical conductivity.[39] Given that the conductivity of the electrode is positively correlated with the performance of the filtering EC into consideration, achieving such a heavy boron-doping concentration in BDD film is crucial for advancing the development of BDD-based filtering EC.

The BDD film was subsequently etched using the RIE technique with a negative substrate bias of −300 V and an etching time of 6 h to form BDD-NAs electrode. Due to the characterization of the nanoarray, the color of BDD film changed from its original gray to black (Figure S2, Supporting Information). As shown in **Figure 1d-e**, BDD-NAs film is strictly composed of vertical-oriented diamond nanoarrays, and the heights of BDD-NAs are 7.0 μm, respectively. Additionally, the nanoarray height of BDD-NAs can be will adjusted by tunning the etching time of the RIE process (Figure S3, Supporting Information). The high-resolution SEM images shows that the width of nanoarray is ~50 nm and the array pitch is 50~200 nm (Figure S4, Supporting Information). Raman spectroscopy was carried out to characterize the crystal quality and boron concentration of BDD-NAs electrodes. As shown in **Figure 1f**, three BDD-related features are observed in the Raman spectrum of each electrode, where two broad bands around 400-500 cm^{-1} and 1100-1200 cm^{-1} are related to boron-doping of diamond, the shoulder peak approximately 1300 cm^{-1} is assigned as T_{2g} mode of diamond.[40] The band position and shape of above three bands are highly related to the

boron doping level. Thus, boron doping degree can be evaluated by fitting these bands. Specifically, the boron concentration in BDD can be further calculated by deconvoluting the Raman band around 400-500 cm^{-1} (Figure S5, Supporting Information). The calculated boron concentration in BDD is 3.44×10^{21} cm^{-3}, comparable to the boron concentration value of obtained from XPS spectra (5.01×10^{21} cm^{-3}), thus far verifying the heavy boron doping degree in our BDD and BDD-NAs. Besides that, the weak intensity of the band at 1550 cm^{-1} related to non-diamond carbon demonstrates that the BDD film exhibits excellent crystallization quality, with no obvious evidence of non-diamond carbon formation during BDD growth. Importantly, the Raman features of BDD-NAs electrodes are almost unchanged compared to that of BDD, revealing that the classical BDD property including wide potential window and electrochemical stability probably retain in BDD-NAs electrode. Based on the above SEM images and Raman spectra, it can be seen that the BDD-NAs films obtained by etching still maintain the typical BDD spectral characteristics, and have vertically oriented porous structures with adjustable array height.

The stable potential window and the electrochemical performances of BDD and BDD-NAs were investigated in a three-electrode system with 1 M Na_2SO_4 aqueous electrolyte. The stable potential window is determined by linear sweep voltammetry (LSV) curves as shown in **Figure 1g-h**. On the criterion of a threshold current density of 0.5 mA/cm^2, the stable potential window of BDD and BDD-NAs is determined to be 3.60 and 2.93 V, respectively. It is important to note that the wide electrochemical window of BDD is attributed to its micron-sized crystals and the excellent crystallization quality. Meanwhile, the slight reduce in the stable potential window of BDD-NAs can be attributed to the surface defects formed during the RIE process [41]. These stable potential windows of BDD and BDD-NAs are obviously wider with other reported electrode materials, [42-44] suggesting the remarkable advantages of BDD and BDD-NAs in building wide workable window capacitors (Figure S6, Supporting Information). This indicates that BDD-NAs retains the wide potential window characteristic of BDD which is essential to build wide workable window capacitors. Additionally, benefiting from an enlarged surface area provided by the nanoarray structure, the capacitive current is enhanced as shown in cyclic voltammetry (CV) curves of BDD-NAs compared with that of BDD (**Figure 1i**). Correspondingly, the capacitance density of BDD-NAs according to the CV curve of the three-electrode system is 547.4 $\mu F/cm^2$, much higher than that of BDD (3.1 $\mu F/cm^2$).

2.2. High-frequency electrochemical performances of the EC based on BDD-NAs electrode

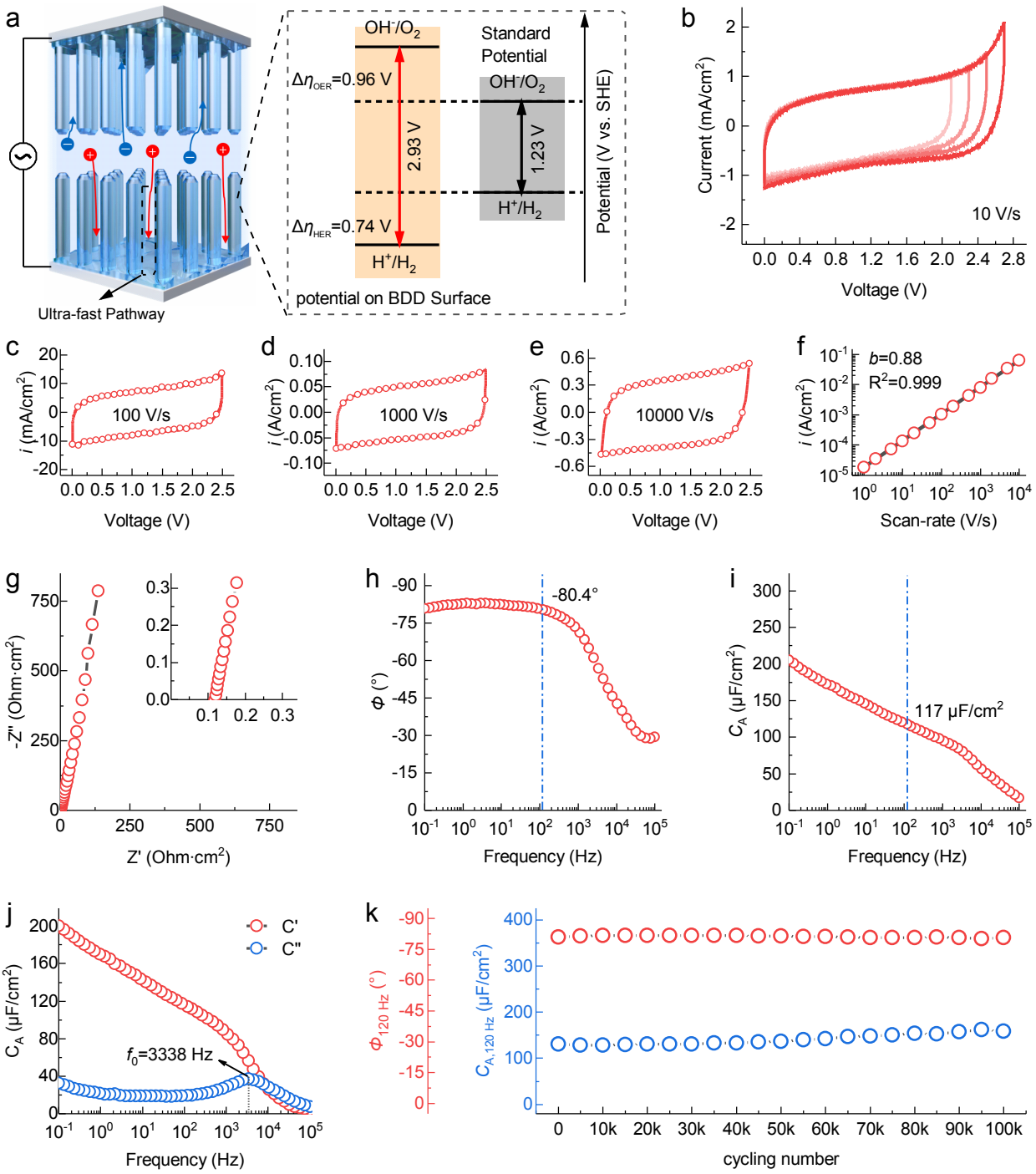

Figure 2. High-frequency electrochemical performances of BDD-NAs-EC. (a) schematic illustrations of the structure of EC and the stable window of BDD/aqueous electrolyte interface; (b) CV curves of EC with varying voltage range of 2.1, 2.3, 2.5 and 2.7 V; (c-e) CV curves at varying

scan rates of 100 V/s (c), 1000 V/s (d), and 10000 V/s (e); (f) The plot of charging current density at 1.25 V versus scan rate; (g) Nyquist plot; (h) Bode phase plot; (i) The plot of specific capacitance versus frequency; (j) The plot of the real and imaginary specific capacitance (C′ and C″) versus frequency at 0 V; (k) The variations of $C_{A,120\ Hz}$ and $\Phi_{120\ Hz}$ during 10^5 cycles charging/discharging processes.

A Symmetric EC unit was constructed utilizing BDD-NAs electrodes to investigated their high-frequency electrochemical performances (noted as BDD-NAs-EC, refer to Figure S7, Supporting Information for details). **Figure 2a** shows the capacitor structure and an illustration of the wide potential window electrochemical interface within BDD-NAs. The high-frequency response characteristics of the EC unit derive from the vertically oriented porous structure of the BDD-NAs electrode, which provides ultrafast transport channels for the electrolyte ions. Additionally, the wide voltage window of the capacitor comes from the fact that the decomposition reaction of the aqueous electrolyte (i.e. OER and HER) on the surface of BDD-NAs has a large overpotential ($\Delta\eta_{OER}$ = 0.96 V, $\Delta\eta_{HER}$ = 0.74 V). The voltage window of BDD-NAs-EC was determined to be 2.5 V by comparing CV curves with different voltage at the scan rate of 10 V/s (**Figure 2b**), indicating the superiority of BDD-NAs in constructing wide-voltage aqueous filtering ECs. **Figure 2c-d** shows the CV curves of the EC unit at the scan rate of 100, 1000, and 10000 V/s, respectively. It can be seen that the EC unit can maintain nearly rectangular CV curve characteristics at ultra-high scan rate of 10,000 V/s benefiting from the ultrafast ion transport pathway in the strictly vertical-oriented nanoarrays of BDD-NAs. Moreover, the discharge current density shows a perfect linear relationship with the scan rate in the range of 1~10000 V s^{-1} (Figure 2f). Besides that, the *b* value is calculated to be 0.88, which is close to 1.0 suggesting an ideal capacitive performance within such a wide scan-rate range.

Electrochemical impedance spectroscopy (EIS) was carried out to investigate the electrochemical performances of the EC unit at discharging state (applied voltage is set to 0 V) over a board frequency range of 10^{-1}~10^5 Hz. As shown in **Figure 2g**, the Nyquist plots exhibit a quasi-vertical line suggesting the ideal-capacitive behavior. As depicted in the inset of **Figure 2g**, the intercept of the plots from the real-impedance axis falls within the range of 0.10-0.15 Ω/cm^2, signifying a low equivalent series resistances (ESR) value for the EC unit. As above-demonstrated, the boron concentration in our BDD-NAs is up to 10^{21} atoms/cm^3, thus resulting in a metal-like electrical conductivity. As a result, the ESR value of the EC unit is equivalent to the reported sp^2-carbon

results. [45-47]

The phase angle and specific capacitance at 120 Hz (i.e., Φ_{120Hz} and $C_{A,\ 120Hz}$) are key performance parameters for filtering ECs. [48-50] The Φ_{120Hz} of the EC unit is determined to be −80.4° though the Bode phase plots (**Figure 2h**), meanings a well capacitive behavior. Besides that, **Figure 2i** shows the plots of specific capacitance versus frequency, in which $C_{A,\ 120Hz}$ of the BDD-NAs electrode is 117 μF/cm^2. Such a $C_{A,120\ Hz}$ value is relatively low compared to those of recently reported results, which can be addressed by architecting other vertical porous BDD materials with higher specific area, such as vertical BDD nanosheets. The plots of specific real (C′) and imaginary (C″) capacitances versus frequency are exhibited in **Figure 2j**. For energy converting, only the C' part of the filtering EC contributes to energy storage and release, while the C" part causes energy dissipation. Therefore, the filtering EC should to work within the frequency range where its C" is less than C' to ensure a high energy conversion efficiency. The time constant (t_0) of the filter EC can be determined by the maximum value of the C"-*f* plots. The maximum frequency (f_0) in the C"-*f* plots is 3338 Hz, and thus t_0 ($t_0=1/f_0$) can be obtained as 299 μs. Such a small t_0 reveals an efficient AC-line filtering ability. Furthermore, C′ is significantly higher than C″ over a board frequency range below 10^3 Hz. The ratio of C″/C′, that is the dissipation factor (DF) of the EC unit, is less than 1 in the frequency range below 7858 Hz, indicating a high energy efficiency within such a board frequency region (Figure S8, Supporting Information). Moreover, the high-frequency electrochemical performance of these filtering EC units can be finely tuned by adjusting the nanoarray height of BDD-NAs (Figure S9, Supporting Information). For instance, the response frequency can be further enhanced above 10^4 Hz using BDD-NAs with a shorter nanoarray height, albeit with a slight reduction in capacitance.

A charge and discharge process of 10^5 cycles was conducted for investigating the stability of the EC unit. The two key parameters of $C_{A,120Hz}$ and $\Phi_{120\ Hz}$ was collected during such a long charging/discharging cycling as shown in **Figure 2k**. Consequently, $C_{A,120Hz}$ is slowly increased during such a process due to the slight activation of the BDD-NAs electrode. Besides that, $\Phi_{120\ Hz}$ remains between −80.2° and −81.8° without any significant attenuation, suggesting the excellent stability of the capacitive surface of BDD-NAs. These results demonstrate the advantages of BDD-NAs electrodes in constructing filtering ECs.

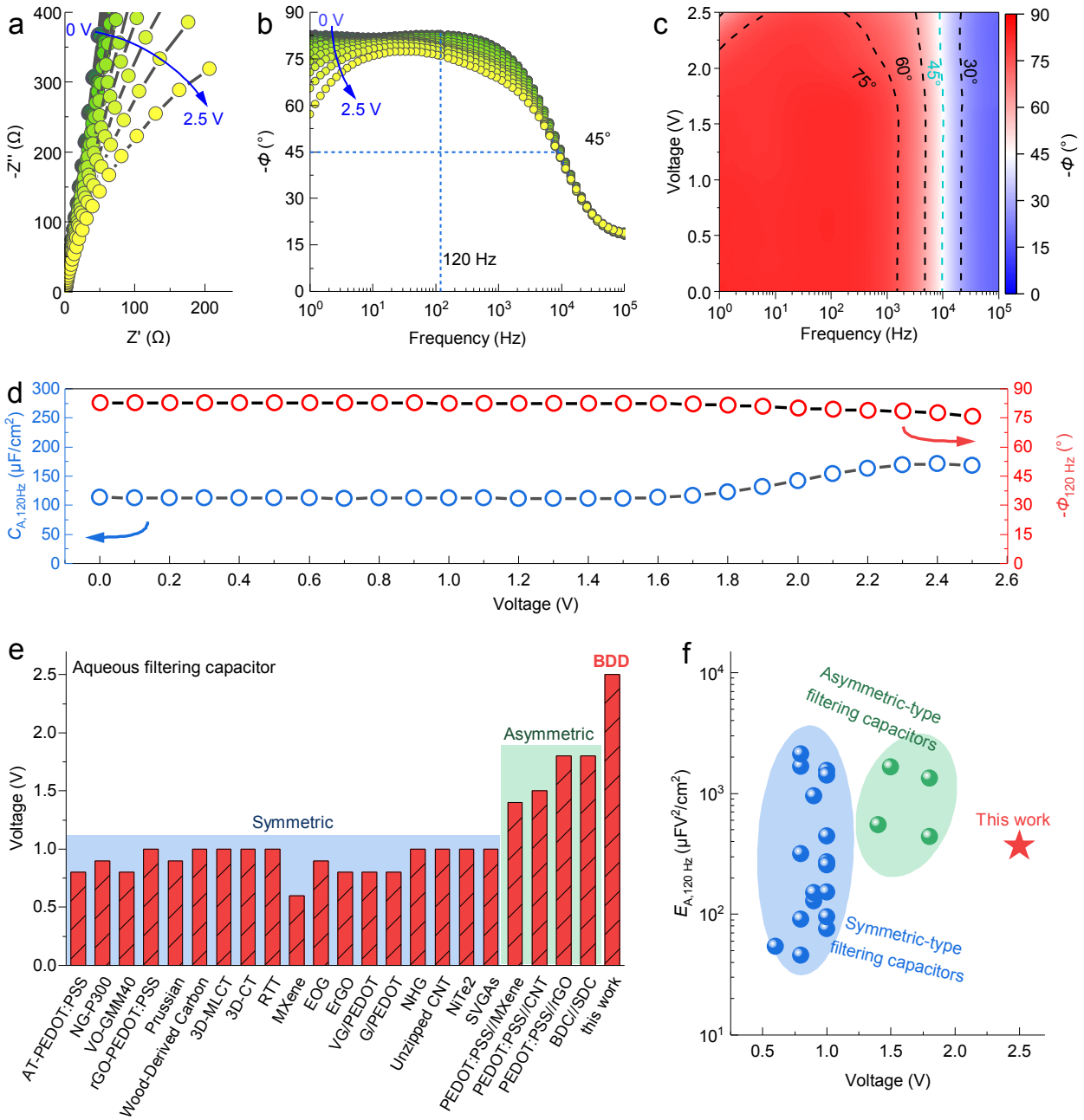

Figure 3. Electrochemical performance of the BDD-NAs-EC unit within the 2.5 V voltage window. (a) Nyquist plots of the EC unit at varying voltages from 0 to 2.5 V; (b) Bode phase plots of the EC unit at varying voltages from 0 to 2.5 V; (c) The contour of Φ in the two-dimension voltage-frequency region; (d) The plots of $\Phi_{120\ Hz}$ and $C_{A,120Hz}$ versus voltage; (e) Comparison of voltage window of BDD-NAs-EC with those if the reported aqueous filtering ECs; (f) $E_{A,\ 120\ Hz}$-voltage plots of BDD-NAs-EC compared with symmetric-type and asymmetric-type aqueous filtering ECs.

As above demonstrated, the BDD-NAs-EC unit delivers a wide workable window of 2.5 V. In this section, the high-frequency performances were further investigated over such a wide voltage range.

The Nyquist plots and Bode plots of the EC unit in the voltage range from 0 to 2.5 V show that as the voltage increases, the Nyquist plot deviates from the vertical line only in the low frequency range, while phase angle experiences a slight decrease solely in this region and remains relatively stable at higher frequencies (**Figure 3a-b**). In order to meet the dual demands of wide voltage window and high-frequency response for the filtering capacitor, it requires that the electrode material maintains ideal capacitance behaviors under both high-frequency excitation and electrochemical polarization, i.e., maintaining its Φ less than −45°. **Figure 3c** presents the Φ distribution of the BDD-NAs-EC unit across frequency-voltage domains, with the $\Phi < -45°$ contour (blue dashed line) higher than 10^3 Hz over the voltage range of 0~2.5 V. This result indicates the effective processing range of such an EC unit for rectified signals with both high frequencies (> 10^3 Hz) and large voltage amplitudes up to 2.5 V. This remarkable high-frequency response originates from ultra-fast ion transport in the vertically oriented nanoarray architecture of BDD-NAs. Meanwhile, due to the exceptional chemical stability and wide potential window characteristics of BDD-NAs, the electrode interface maintains ideal capacitive characteristics even under high voltage polarization states, resulting in minimal changes in its Bode phase plots with varying voltages even up to 2.5 V. As a control, the sp^2 carbon electrode material shows the performance deviating from the ideal polarization surface under high voltage polarization states, ultimately leading to a decline in the high-frequency performance of the device during the charging state (Figure S10, Supporting Information).

The specific capacitance of BDD-NAs-EC unit was further evaluated within the wide voltage window of 2.5 V. The areal specific capacitance (C_A) exhibits a pronounced increase with applied voltage (Figure S11, Supporting Information). This increase is mainly derived from the enhancement of C′ at high voltage state, thus mainly contributes to reversible energy transform rather than energy dissipation (Figure S12, Supporting Information). **Figure 3d** shows the variation results of $C_{A,\ 120\ Hz}$ and $\Phi_{120\ Hz}$ at varying voltage. Similarly, $C_{A,120\ Hz}$ is obviously increased at voltages higher than 2.0 V due to the enhanced surface activity of the high-polarized BDD-NAs electrode. The value of $\Phi_{120\ Hz}$ keep < −80° at varying voltage and only decay slightly when the applied voltage is higher than 2.0 V. This result can be attributed to the minor deviations from ideal capacitive characteristics at the polarized BDD electrode surface even at high voltage state. The results demonstrate that the BDD-NAs-EC maintains its stable high-frequency performance over the wide operational window of 2.5 V, which value is higher than that of other aqueous filtering ECs reported to date (**Figure 3e**).

Combined with the voltage window of 2.5 V, the areal specific energy density of the BDD-NAs-EC at 120 Hz ($E_{A,\ 120\ Hz}$) was calculated to be 365.6 μFV²/cm², which is relatively high among the reported symmetric-type and asymmetric-type aqueous filtering ECs (**Figure 3f** and Table S2, Supporting Information)[3-9,19,23,51-62].

2.3. Filtering performances of the EC based on BDD-NAs electrode

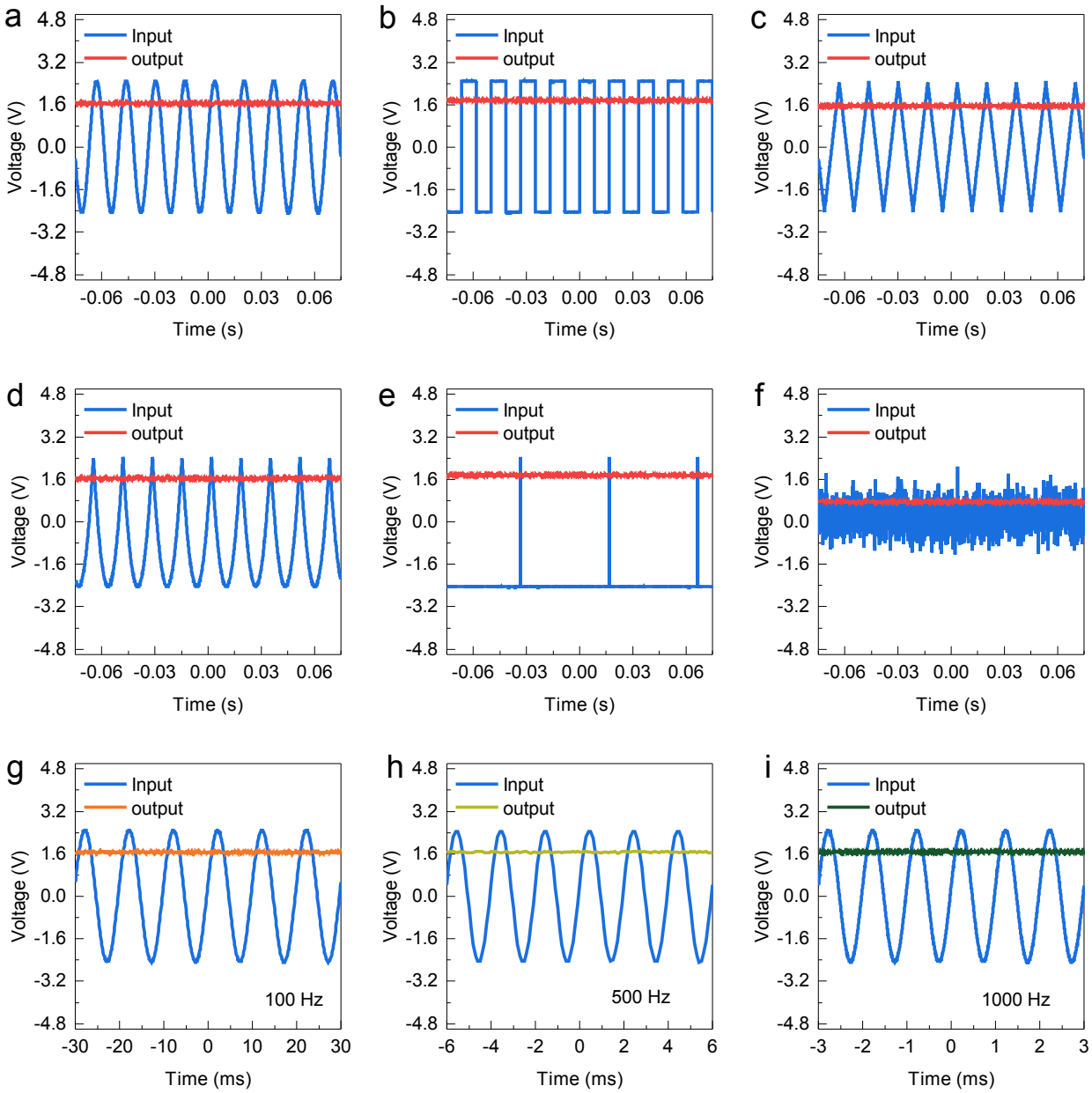

Figure 4. The filtering performance of BDD-NAs-EC unit. The AC inputs are sinusoidal (a), square (b), triangular (c), absorption (d), and pulse waveforms (e), the frequency in (a) to (e) is 60 Hz; (f) The filtering performance for the noise waveform with irregularly high-frequency violent

pulses; (g-i) The frequency of AC inputs are 100 (g), 500 (h) and 1000 Hz (i).

To further verify the filtering performances, a BDD-NAs-EC unit was served as the filtering capacitor assembled into an experimental model rectifier and filter circuit (**Figure S13**). As shown in **Figure 4a**, the EC unit is able to successfully smooth the input rectified signals of 60 Hz sinusoidal AC wave with a peak-to-peak voltage of 5.0 V into constant-voltage DC. The voltage ripple of the obtained DC is ~100 mV comparable to that of a commercial AEC (Figure S14, Supporting Information). Furthermore, the EC unit can well smooth the 60 Hz AC with complex waveforms including square, triangular, absorbed and impulse inputs (**Figure 4b-e**). The output results are constant-voltage DC, which indicates that the EC unit can achieve effective filtering function for complex AC inputs. Besides that, the EC unit is capable of further filtering noise waveforms with irregularly high-frequency violent pulses (**Figure 4f**). This result suggests the great filtering capability of the EC unit for complex AC inputs.

As BDD-NAs-EC ability to operate over a broad frequency-voltage range, its filtering performance was tested in a broad frequency range of 100~1000 Hz. **Figure 4g-i** respectively shows the filtering performance of the EC unit at 100, 500, and 1000 Hz, demonstrating that the EC unit can effectively smooth AC signals with a voltage amplitude of 5.0 V into constant-voltage DC with a small voltage ripple of ~100 mV in such a broad range of 100 to 1000 Hz. The output ripple voltage, obtained after smoothing AC signals ranging from 60 to 1000 Hz, does not increase significantly with the frequency, which is benefitted from the high-frequency response capability of the strictly vertical-oriented nanoarrays structure in BDD-NAs (Figure S15, Supporting Information). The BDD-NAs-EC maintains excellent high-frequency electrochemical even when connected in series configurations (Figure S16, Supporting Information), thus leading to excellent filtering performance in smoothing the AC input with 10 V voltage amplitude (Figure S17, Supporting Information). Combined with the above powerful filtering performance for AC input signals with complex waveforms, high frequency and high voltage amplitude, EC has excellent application prospects in renewable energy conversion with intermittent and fluctuating, high frequency and noise reduction circuit units in power electronics.

3. Conclusion

Boron-doped diamond nanoarrays (BDD-NAs) were prepared for developing aqueous filtering electrochemical capacitor (EC) with a wide voltage window and a thousand-Hertz response. The EC based on BDD-NAs exhibits a wide workable window up to 2.5 V and a high-frequency response with f_0= 3338 Hz. Additionally, this EC delivers a capacitive phase angle of −80.4° and an energy density of 365.6 μFV^2/cm^2 at 120 Hz. Assembled into an experimental filtering circuit, such a filtering EC unit can filter AC line with the frequency range of 60-1000 Hz and different waveforms. Considering excellent filtering capabilities for AC input signals featuring complex waveforms, high frequency, and high voltage amplitude, this capacitor exhibits exceptional potential in the field of renewable energy conversion, particularly dealing with intermittent and fluctuating power sources, as well as high-frequency noise reduction circuit units in power electronics. Above all, our work demonstrates a high-performance filtering capacitor design that simultaneously achieves wide voltage windows and fast frequency response, overcoming critical integration and miniaturization challenges in next-generation electronics.

Supporting Information

Supporting Information is available from the Wiley Online Library or from the author.

Acknowledgements

This work was supported by the Pilot Scale Testing Project of Liaoning Province (2022JH24/10200033), "Jie Bang Gua Shuai" Key Technologies R & D Program of Liaoning Province (2021JH1/10400031), the National Nature Science Foundation of China (52173242), Guangdong Basic and Applied Basic Research Foundation (2019B1515120005), Shenzhen Science and Technology Planning Project (JCYJ20200109115424940).

Data availability

Data will be made available on request.

Received: ((will be filled in by the editorial staff))
Revised: ((will be filled in by the editorial staff))
Published online: ((will be filled in by the editorial staff))

References

[1] Wang F, Wu X, Yuan X, Liu Z, Zhang Y, Fu L, et al. Latest advances in Electrochemical capacitors: from new electrode materials to novel device designs. *Chem. Soc. Rev.* **2017**, 22, 6816.

[2] Park J, Kim W. History and perspectives on ultrafast electrochemical capacitors for AC line filtering. *Adv. Energy Mater.* **2021**,11, 2003306.

[3] Hu Y, Wu M, Chi F, Lai G, Li P, He W, et al. Ultralow-resistance electrochemical capacitor for integrable line filtering. *Nature*. **2023**, 624, 74.

[4] Han F, Qian O, Meng G, Lin D, Chen G, Zhang S, et al. Structurally integrated 3D carbon tube grid–based high-performance filter capacitor. *Science*. **2022**, 377, 1004.

[5] Wu M, Chi F, Geng H, Ma H, Zhang M, Gao T, et al. Arbitrary waveform AC line filtering applicable to hundreds of volts based on aqueous electrochemical capacitors. *Nat. Commun*. **2019**, 10, 2855.

[6] Li Z, Wang XP, Zhao LY, Chi FY, Gao C, Wang Y, et al. Aqueous hybrid electrochemical capacitors with ultra-high energy density approaching for thousand-Volts alternating current line filtering. *Nat. Commun.* **2022**, 13, 6359.

[7] Chen G, Han F, Lin D, Zhang S, Pan Q, Shao C, et al. Three-dimensional multi-layer carbon tube

electrodes for AC line-filtering capacitors. *Joule*. **2024**, 8, 1080.

[8] Lim J, Maiti UN, Kim NY, Narayan R, Lee WJ, Choi DS, et al. Dopant-specific unzipping of carbon nanotubes for intact crystalline graphene nanostructures. *Nat. Commun*. **2016**, 7, 10364.

[9] Wang C, Vi-Tang S, Qu S, He Z, Peng B, Chang X, et al. Design of efficient, reliable, and wide-band filter electrochemical capacitors via matching positive with negative electrodes. *Joule*. **2024**, 8, 764.

[10] Wu ZS, Liu Z, Parvez K, Feng X, Mullen K. Ultrathin printable graphene Electrochemical capacitors with AC line-filtering performance. *Adv. Mater.* **2015**, 24, 3669.

[11] Miller JR, Outlaw RA, Holloway BC. Graphene double-layer capacitor with AC line-filtering performance. *Science*. **2010**, 329, 1637.

[12] Chi F, Li C, Zhou Q, Zhang M, Chen J, Yu X, et al. Graphene-Based Organic Electrochemical Capacitors for AC Line Filtering. *Adv. Energy Mater.* **2017**, 7, 1700591.

[13] Cai M, Outlaw RA, Butler SM, Miller JR. A high density of vertically-oriented graphenes for use in electric double layer capacitors. *Carbon.* **2012**, 50, 5481.

[14] Premathilake D, Outlaw RA, Parler SG, Butler SM, Miller JR. Electric double layer capacitors for AC-line filtering made from vertically oriented graphene nanosheets on aluminum. *Carbon.* **2017**, 111, 231.

[15] Ren G, Pan X, Bayne S, Fan Z. Kilohertz ultrafast electrochemical capacitors based on perpendicularly-oriented graphene grown inside of nickel foam. *Carbon.* **2014**, 71, 94.

[16] Bo Z, Xu C, Yang H, Shi H, Yan J, Cen K, et al. Hierarchical, Vertically-oriented carbon nanowall foam supercapacitor using room temperature ionic liquid mixture for AC line filtering with ultrahigh energy density. *ChemElectroChem*. **2019**, 6, 2167.

[17] Wang L, Li Z, Song M, Xu C, Liu Z, Jia S, et al. Enabling directional ion transport over graphene electrode surfaces for kilohertz electrochemical capacitors. *Electrochim. Acta.* **2021**, 368, 137561.

[18] Premathilake D, Outlaw RA, Quinlan RA, Parler SG, Butler SM, Miller JR. Fast response carbon-black-coated vertically-oriented graphene electric double layer capacitors. *J. Electrochem. Soc.* **2018**, 165, 924.

[19] Xu S, Wen Y, Chen Z, Ji N, Zou Z, Wu M, et al. Vertical graphene arrays as electrodes for ultra-high energy density AC line-filtering capacitors. *Angew Chem. Int. Ed.* **2021**, 60, 24505.

[20] Yverick Ranom X, Linda F. Nazar. Carbon nanotube-based Electrochemical capacitors with

excellent AC line filtering and rate capability via improved interfacial impedance. *ACS Nano*. **2015**, 9, 7248.

[21] Han ZJ, Huang C, Meysami SS, Piche D, Seo DH, Pineda S, et al. High-frequency Electrochemical capacitors based on doped carbon nanostructures. *Carbon*. **2018**, 126, 305.

[22] Yoo Y, Kim MS, Kim JK, Kim YS, Kim W. Fast-response Electrochemical capacitors with graphitic ordered mesoporous carbons and carbon nanotubes for AC line filtering. *J. Mater. Chem. A*. **2016**, 4, 5062.

[23] Wen Y, Chen H, Wu M, Li C. Vertically oriented MXene bridging the frequency response and capacity density gap for AC filtering pseudocapacitors. *Adv. Funct. Mater.* **2022**, 32, 211613.

[24] Gund GS, Park JH, Harpalsinh R, Kota M, Shin JH, Kim T-i, et al. MXene/polymer hybrid materials for flexible AC-filtering electrochemical capacitors. *Joule*. **2019**, 3, 164.

[25] Xia M, Liu Q, Ning J, Wang D, Hao Y, Zhang J. Photon-beam-inducing synthesis of a tunable porous graphene/$Ti_3C_2T_x$ heterostructure for energy conversion-storage system. *Nanotechnology*. **2024**, 35, 425401.

[26] Zhao M, Qin Y, Wang X, Wang L, Jin Q, Song M, et al. PEDOT:PSS/ketjenblack holey nanosheets with ultrahigh areal capacitance for kHz AC line-filtering micro-Electrochemical capacitors. *Adv. Funct. Mater.* **2023**, 34, 2313495.

[27] Chi F, Li C, Zhou Q, Zhang M, Chen J, Yu X, et al. Graphene-based organic electrochemical capacitors for AC line filtering. *Adv. Energy Mater*. **2017**, 7, 1700591.

[28] Kang YJ, Yoo Y, Kim W. 3V solid-state flexible Electrochemical capacitors with ionic-liquid-based polymer gel electrolyte for AC line filtering. *ACS Appl. Mater. Interfaces.* **2016**, 8, 13909.

[29] Yoo Y, Park J, Kim M-S, Kim W. Development of 2.8 V Ketjen black Electrochemical capacitors with high rate capabilities for AC line filtering. *J. Power Sources.* **2017**, 360, 383.

[30] Park J, Lee J, Kim W. Water-in-salt electrolyte enables ultrafast Electrochemical capacitors for AC line filtering. *ACS Energy Letters*. **2021**, 6, 769.

[31] Chi F, Hu Y, He W, Weng C, Cheng H, Li C, et al. Graphene ionogel ultra-fast filter supercapacitor with 4 V workable window and 150 degrees operable temperature. *Small.* **2022**, 18, 2200916.

[32] Yang NJ, Yu SY, Macpherson JV, Einaga Y, Zhao HY, Zhao GH, et al. Conductive diamond: synthesis, properties, and electrochemical applications. *Chem. Soc. Rev.* **2019**, 48, 157.

[33] Martin HB, Argoitia A, Landau U, Anderson AB, Angus JC. Hydrogen and oxygen evolution on

boron-doped diamond electrodes. *J. Electrochem. Soc.* **1996**, 143, 133.

[34] Hupert M, Muck A, Wang R, Stotter J, Cvackova Z, Haymond S, et al. Conductive diamond thin-films in electrochemistry. *Dia. Relat. Mater*. **2003**, 12, 1940.

[35] Gao F, Nebel CE. Diamond-based Electrochemical capacitors: realization and properties. *ACS Appl. Mater. Interfaces.* **2016**, 8, 28244.

[36] Gao F, Wolfer MT, Nebel CE. Highly porous diamond foam as a thin-film micro-supercapacitor material. *Carbon.* **2014**, 80, 833.

[37] Wang J, He ZB, Tan XL, Wang T, Liu L, He XS, et al. High-performance 2.6 V aqueous symmetric supercapacitor based on porous boron-doped diamond via regrowth of diamond nanoparticles. *Carbon.* **2020**, 160, 71.

[38] Lu Z, Huang N, Zhai Z, Chen B, Liu L, Song H, et al. Integration of 3D interconnected porous microstructure and high electrochemical property for boron-doped diamond by facile strategy. *J. Mater. ECi. Technol.* **2022**, 105, 26-35.

[39] Blase X, Bustarret E, Chapelier C, Klein T, Marcenat C. Superconducting group-IV semiconductors. *Nat. Mater.* **2009**, 8, 375.

[40] Bernard M, Deneuville A, Muret P. Non-destructive determination of the boron concentration of heavily doped metallic diamond thin films from Raman spectroscopy. *Dia. Relat. Mater.* **2004**, 13, 282.

[41] Kondo T, Kodama Y, Ikezoe S, Yajima K, Aikawa T, Yuasa M. Porous boron-doped diamond electrodes fabricated via two-step thermal treatment. Carbon. 2014, 77, 783.

[42] Heard DM, Lennox AJJ. Electrode Materials in Modern Organic Electrochemistry. *Angew Chem Int Ed.* **2020**,59, 18866.

[43] Qu K, Zheng Y, Jiao Y, Zhang X, Dai S, Qiao SZ. Polydopamine Inspired, Dual Heteroatom Doped Carbon Nanotubes for Highly Efficient Overall Water Splitting. *Advanced Energy Materials.* **2016**, 7, 1602068.

[44] Chen X, Zhai X, Hou J, Cao H, Yue X, Li M, et al. Tunable nitrogen-doped delaminated 2D MXene obtained by NH_3/Ar plasma treatment as highly efficient hydrogen and oxygen evolution reaction electrocatalyst. *Chemical Engineering Journal*. **2021**, 420, 129832.

[45] Chen B, Huang N, Zhai Z, Zhang C, Liu L, Yang B, et al. Enhancing interfacial capacitance by boron doping in vertically porous carbon toward high-performance AC-line filtering electrochemical capacitors. *Small.* **2024**, 13, 2310523.

[46] Zhou Q, Zhang M, Chen J, Hong JD, Shi G. Nitrogen-doped holey graphene film-based ultrafast electrochemical capacitors. *ACS Appl. Mater. Interfaces.* **2016**, 8, 20741.

[47] Zhang M, Dong K, Saeedi Garakani S, Khorsand Kheirabad A, Manke I, Wu M, et al. Bridged carbon fabric membrane with boosted performance in AC line-filtering capacitors. *Adv. Sci.* 2022, 9, 2105072.

[48] Fan ZY, Islam N, Bayne SB. Towards kilohertz electrochemical capacitors for filtering and pulse energy harvesting. *Nano Energy*. **2017**, 39, 306.

[49] Tang H, Tian Y, Wu Z, Zeng Y, Wang Y, Hou Y, et al. AC line filter electrochemical capacitors: materials, morphology, and configuration. *Energy Environ. Mater.* **2022**, 5, 1060.

[50] Xu S, Wu M, Zhang J. Ultrafast electrochemical capacitors with carbon related materials as electrodes for AC line filtering. *Chemistry*. **2022**, 28, 202200237.

[51] Jiang Q, Kurra N, Maleski K, Lei Y, Liang H, Zhang Y, et al. On Chip MXene Microsupercapacitors for AC Line Filtering Applications. Adv. Energy Mater. **2019**, 9, 1901061.

[52] Zhao D, Chang W, Lu C, Yang C, Jiang K, Chang X, et al. Charge transfer salt and graphene heterostructure-based micro-supercapacitors with alternating current line-filtering performance. *Small.* **2019**, 15, 1901494.

[53] Zhang M, Wang W, Tan L, Eriksson M, Wu M, Ma H, et al. From wood to thin porous carbon membrane: Ancient materials for modern ultrafast electrochemical capacitors in alternating current line filtering. *Energy Storage Mater.* **2021**, 35, 327.

[54] Li W, Azam S, Dai G, Fan Z. Prussian blue based vertical graphene 3D structures for high frequency electrochemical capacitors. *Energy Storage Mater.* **2020**, 32, 30.

[55] Zhang M, Yu XW, Ma HY, Du WC, Qu LT, Li C, et al. Robust graphene composite films for multifunctional electrochemical capacitors with an ultrawide range of areal mass loading toward high-rate frequency response and ultrahigh specific capacitance. *Energy Environ Sci.* **2018**, 11, 559.

[56] Sheng KX, Sun YQ, Li C, Yuan WJ, Shi GQ. Ultrahigh-rate supercapacitors based on electrochemically reduced graphene oxide for AC line-filtering. *Scientific Reports.* **2012**, 2, 247.

[57] Islam N, Warzywoda J, Fan ZY. Edge-oriented graphene on carbon nanofiber for high-frequency supercapacitors. *Nano-Micro Letters*. **2018**, 10, 9.

[58] Zhou Q, Zhang M, Chen J, et al. Nitrogen-doped holey graphene film-based ultrafast

electrochemical capacitors. *ACS Appl. Mater. Interfaces,* **2016**, 8, 20741.

[59] Hu Y, Li P, Lai G, Lu B, Wang H, Cheng H, et al. Separator with high ionic conductivity enables electrochemical capacitors to line-filter at high power. *Nat. Commun.* **2025**, 16, 2772.

[60] Zhang M, Zhou QQ, Chen J, Yu XW, Huang L, Li YR, et al. An ultrahigh-rate electrochemical capacitor based on solution-processed highly conductive PEDOT:PSS films for AC line-filtering. *Energy Environ Sci*. **2016**, 9, 2005.

[61] Chang Y, Han G, Fu D, Liu F, Li M, Li Y, et al. Paper-like N-doped graphene films prepared by hydroxylamine diffusion induced assembly and their ultrahigh-rate capacitive properties. *Electrochim Acta.* **2014,** 115, 461.

[62] Tang H, Xia K, Lu J, Fu J, Zhu Z, Tian Y, et al. $NiTe_2$-based electrochemical capacitors with high-capacitance AC line filtering for regulating TENGs to steadily drive LEDs. *Nano Energy*. **2021**, 84, 105931.

Table of Contents

Aqueous AC-Line Filtering Electrochemical Capacitors Featuring 2.5-V Voltage Window and Kilohertz Response Using Boron-Doped Diamond Nanoarrays

*Bin Chen, Zhaofeng Zhai, Chuyan Zhang, Junyao Li, Shuailong Zheng, Lusheng Liu, Wenjun Zhang, Xin Jiang, Yang Yang, * Nianjun Yang, * Nan Huang, **

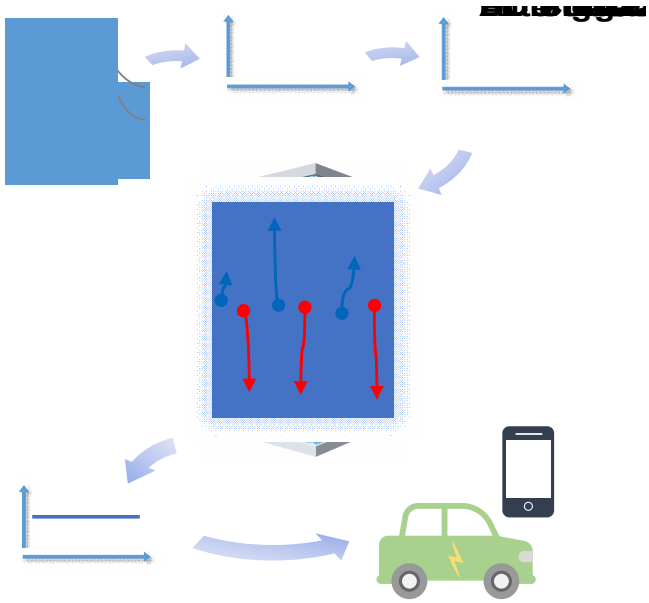

Boron-doped diamond nanoarrays (BDD-NAs) is prepared for developing aqueous filtering electrochemical capacitor (EC) with a wide workable window up to 2.5 V and a high-frequency response with f_0= 3338 Hz. Such superior electrochemical performance positions BDD-NAs based EC as highly promising candidates for power electronics applications, particularly in AC-DC conversion systems for power grids and renewable energy integration.